Reprogrammable Braille on an elastic shell

Jun Young Chung[a], Ashkan Vaziri[b], and L. Mahadevan[c,1]

[a]Paulson School of Engineering and Applied Sciences, Wyss Institute for Biologically Inspired Engineering, Harvard University, Cambridge, MA 02138; [b]Department of Mechanical and Industrial Engineering, Northeastern University, Boston, MA 02115; and [c]Paulson School of Engineering and Applied Sciences, Wyss Institute for Biologically Inspired Engineering, Department of Physics, Harvard University, Cambridge, MA 02138

Edited by William D. Nix, Stanford University, Stanford, CA, and approved June 4, 2018 (received for review December 21, 2017)

We describe a minimal realization of reversibly programmable matter in the form of a featureless smooth elastic plate that has the capacity to store information in a Braille-like format as a sequence of stable discrete dimples. Simple experiments with cylindrical and spherical shells show that we can control the number, location, and the temporal order of these dimples, which can be written and erased at will. Theoretical analysis of the governing equations in a specialized setting and numerical simulations of the complete equations allow us to characterize the phase diagram for the formation of these localized elastic states, elastic bits (e-bits), consistent with our observations. Given that the inherent bistability and hysteresis in these low-dimensional systems arise exclusively due to the geometrical-scale separation, independent of material properties or absolute scale, our results might serve as alternate approaches to small-scale mechanical memories.

programmable matter | elastic shell | Braille | mechanical memory | multistability

The main requirement for memory is a dynamical system with multiple metastable states. This is usually realized using biochemical means in nature and electromagnetic means in technology. Memories are typically discrete and thus, impose certain requirements on the substrate on which they are stored, foremost among them being the presence of a lattice-like structure at each site of which the system has access to multiple configurations. For example, in biological systems, discrete chemical bonds (e.g., DNA) or synapses (e.g., neurons) encode memory at molecular and cellular scales (1), while in technological systems, analogs arise as dips and flats in CDs, discrete spins in magnetic memories and other electromagnetic storage devices, multistable mechanical memory elements in cantilever or biomorph arrays, and phase-changing materials in memristors (2–5). All of these systems have a discrete set of possible states as required by any memory. In a spatial setting, this raises the question of whether the presence of a lattice is essential for the spatial encoding of information. Theoretical work on localized patterns in spatially extended dynamical systems (6–9) suggests that this is not the case, but there is a paucity of examples of how this might be actually realized in a practical setting. The advantages of a lattice-free physical memory are that they allow for a realization of programmable matter that requires little in terms of infrastructure and yet, is capable of storing high density memories. Additionally, if it is possible to erase these memories easily, the added benefit of read–write memories is obvious.

Here, we show that a thin curved elastic shell can be used to realize a programmable read–write memory that is analogous to lattice-free Braille. Our starting point is the observation that an elastic shell is well-known to exhibit bistability in certain geometries and under certain loading conditions (10): for example, one-half of a tennis ball can be stable in its rest state as well as in a partially everted state as can mechanical toys, such as a snap bracelet (11, 12). By considering spatially extended versions of these toys, we show that a qualitatively distinct feature arises: the potential for the presence of localized elastic dimples that can form almost anywhere in the system (away from a boundary) in the absence of any underlying discrete lattice. This allows us to encode programmable elastic bits akin to lattice-free Braille that naturally serve as a mechanical memory in an otherwise featureless substrate.

Experiments

A common realization of this is shown in Fig. 1; when a fruit bowl made of plastic is pushed transiently with a finger along its curved rim, the shell pops locally and forms a stable localized dimple that can be maintained without any external forces. Different configurations consisting of interacting and noninteracting localized dimples can be shaped by indenting the fruit bowl in different locations along its periphery, and the dimples can be easily made to disappear by unpopping them. Thus, we see that it is possible to have localized structures with number and position that are controllable on an otherwise featureless continuum. These "bits" are the basis for a reprogrammable spatial memory in a medium without an underlying lattice. While the simplicity of the process is beguiling, the complex geometry of the fruit bowl raises the challenge of whether it is possible to simplify things still further.

Since elastic bistability occurs only in curved shells, the simplest exemplar of which is a cylindrical shell, we created a segment of one by constraining a long strip of relatively thin elastic sheet (length L, width a, and thickness t; $L \gg a \gg t$) between two parallel guide rails that are gently brought together as shown in Fig. 2*A* to create a shallow cylindrical arch (*Materials and Methods* has details). Under certain loading conditions, this long, weakly curved cylindrical shell can exhibit two stable states (Fig. 2*B*). When the arch is pushed gently with an indenter, the shell deforms over a length comparable with its width, relatively locally, but the shell recovers its original shape when the force is released, as shown in Fig. 2*C* (i.e., the system does not

Significance

Generically, memory requires a dynamical system that has multiple metastable states or in disordered systems, broken ergodicity. In living systems, memory is encoded biochemically, while in engineered systems, it is encoded electromagnetically. However, it can be realized using other means as well. We show how an otherwise featureless long cylindrical elastic plate can, when loaded appropriately, serve to store elastic bits, localized dimples and bumps that can be written and erased at will anywhere along it. Using experiments, theory, and computations, we determine the conditions under which we can write on such a linear device using a mechanical stylus and suggest that this might serve as the basis for small-scale mechanical memories.

Author contributions: L.M. designed research; J.Y.C., A.V., and L.M. performed research; J.Y.C., A.V., and L.M. contributed new reagents/analytic tools; J.Y.C., A.V., and L.M. analyzed data; and J.Y.C., A.V., and L.M. wrote the paper.

The authors declare no conflict of interest.

This article is a PNAS Direct Submission.

[1]To whom correspondence should be addressed. Email: lmahadev@g.harvard.edu.

This article contains supporting information online at www.pnas.org/lookup/suppl/doi:10.1073/pnas.1722342115/-/DCSupplemental.

Published online July 2, 2018.

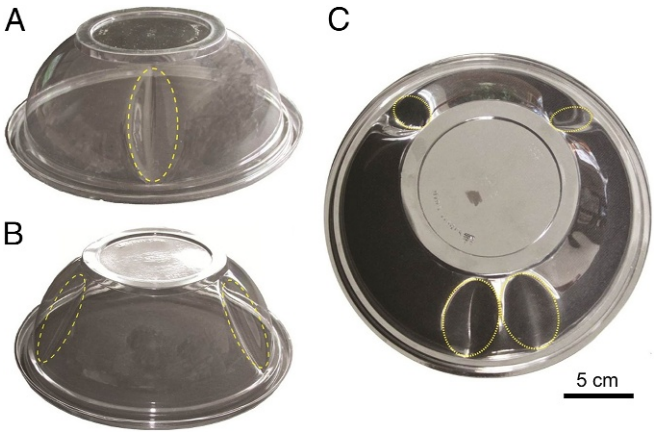

Fig. 1. Localized dimples in a doubly curved shell. (*A*) A single dimple formed by poking an inverted plastic fruit bowl at the location of dimple formation. The fruit bowl is 0.5-mm thick, and it has a diameter of 22 cm and a height of 8 cm. (*B*) Two dimples formed by poking the bowl at two points that are far from each other relative to the dimple width (wavelength). If the points are close, the poking leads to formation of a single or double dimple. (*C*) Two single dimples and one double dimple. The dimple wavelength and amplitude are ∼5 and 1 cm, respectively.

support multiple states and is monostable). However, when the cylindrical arch is sufficiently compressed axially and the same experiment is carried out again, we see a qualitatively distinct behavior (Fig. 2*D*). Now, although in the absence of any indentation force, the cylindrical feature remains uniform axially, when compressed sufficiently, a localized dimple forms that persists even when the force is removed (i.e., we have bistability).

The location of the dimple can be controlled by the location of the indenter, and furthermore, we can write multiple bits that are separate and noninteracting as shown in Fig. 2*E*, *Left*. As the axial compressive strain is increased, we also see that other configurations such as dimple doublets (much like those on the fruit bowl in Fig. 1*C*) and those with an even larger number of conjoined dimple configurations can be created (Fig. 2*E*, *Right*). The range over which these different configurations of dimples persist is determined by bounds on the axial strain on the cylindrical arch and suggests a simple mechanism to tune the spatial persistence of these dimples that are reminiscent of Braille but with an important qualitative difference—-they do not require a template lattice. Furthermore, the patterns are all erasable by simply relieving the axial compressive strain (Fig. 2*D*, *Left*), showing that, although the system is nonlinear, it is geometrically controlled—-material nonlinearities are irrelevant for the observed behavior. Our qualitative experiments with singly and doubly curved shells clearly show that it is possible to have reprogrammable mechanical memories with the simplest of ingredients—-a thin elastic sheet that is preloaded and geometrically curved.

Analysis

Theory. To understand our results, we start with the equations of equilibrium for a thin long plate (thickness t, width W, and length L; $t/W \ll 1$, $W/L \ll 1$) that are given by (10):

$$\begin{aligned} B\nabla^4 w &= p + [w, \phi] \\ \frac{1}{S}\nabla^4 \phi &= -\frac{1}{2}[w, w] \end{aligned} \quad \textbf{[1]}$$

Here, $w = w(x, y)$ is the deflection of the shell relative to its rest state; $\phi = \phi(x, y)$ is the Airy stress function (with derivatives that yield the components of the depth-integrated in-plane stresses); $B = Et^3/12(1-\sigma^2)$ and $S = Et$ are the bending and stretching stiffness of the curved surface made of material with Young's modulus E and Poisson ratio σ, respectively; p is the applied transverse pressure; and $[f(x, y), g(x, y)] = f_{,xx}\, g_{,yy} - f_{,xy}\, g_{,xy}$ where $A_{,b} = \partial A/\partial b$, etc. The first equation corresponds to the balance of forces transverse to the shell (generalizing Laplace's law), while the second one enforces strain compatibility in the tangent plane (and is the mechanical equivalent of the Gauss–Codazzi compatibility relations for a surface).

One can formally write Eq. **1** as a single nonlocal equation by integrating the second equation and substituting into the first equation, so that $B\nabla^4 w = p - \frac{S}{2}\left[w, \nabla^{-4}\left([w, w]\right)\right]$, where we see the presence of a cubic nonlinearity that arises purely from geometric considerations. To formalize this further in the context of a long narrow plate as described in our experiments, we assume that, in the lateral direction, the plate is deformed into a shallow cylinder with an axis parallel to the y axis with boundary conditions $w(0, y) = 0 = w(W, y) - \Delta$; $w_{,xx}(0, y) = w_{,xx}(W, y)$. This immediately leads to the form of the shell given by a simple cylindrical deformation of the form $w(x, y) = f(y) \sin kx$, where $k = \pi/W$. We note that there are boundary layers near the longitudinal ends of the shell of size $(tW^{3/2}\Delta^{-1/2})^{1/2}$, which we can ignore if they are small compared with the length of the plate L. Then, following (13), we may write the thickness-averaged lateral compressive stress as $\phi_{,yy} = Et[-\Delta/W + (f^2k^2/4)(1 + \cos 2kx)]$, which on substituting into the first equation in Eq. **1**, multiplying by $\sin kx$, and integrating across the width of the plate W, yields a width-averaged Galerkin approximation to the coupled partial differential equations (Eq. **1**) that reads (13)

$$Bf_{,yyyy} - 2Bk^2 f_{,yy} + k^4 f = -Sk^2(\Delta/W + f^2k^2/4)f + P, \quad \textbf{[2]}$$

where $P(y) = \int_0^W p(x, y) \sin kx\ dx$. As noted before, this equation is the time-independent Swift–Hohenberg (S-H) equation (14):

$$(1 + \partial_{yy})^2 u - ru + u^3 - \eta = 0, \quad \textbf{[3]}$$

a paradigmatic pattern-forming partial differential equation with solutions that correspond to spatially localized states (9, 14, 15) that has served as a model to study how memory and information may be stored in dynamical systems (7, 8, 16). The homogeneous counterpart of Eq. **3** can be seen to have two stable solutions, while the second- and fourth-order diffusion terms associated allow for complex spatial patterns, and the constant η breaks the $u \to -u$ symmetry. The coexistence of a periodic pattern and a homogeneous pattern combined with spatial reversibility for the same value of the parameters implies the presence of a virtual lattice that serves to pin the localized structures (6, 17) that are the hallmark of memory. Although the generalization of this argument rigorously to the 2D S-H equation remains an open question (9), numerical simulations of the 2D S-H equation show the existence of localized solutions. This suggests that the complete plate (and shell) equations are also capable of nonlinear localized patterns in addition to the well-known global patterns associated with wrinkling, folding, and dimpling (18).

Simulations. To quantify the patterns associated with these loaded elastic shells, we use a numerical model of a long, weakly curved cylindrical shell implemented using the finite element method in ABAQUS, a commercial finite element package, with the following material parameter values: Young's modulus E = 100 GPa and Poisson ratio σ = 0.3 (*Materials and Methods* has details). We assume that the shell is pinned along its long edges and subject to a weak longitudinal compression and transverse indentation loading as shown in Fig. 3*A* in two stages: first, the shell is compressed uniformly by a finite amount, and second, a localized transverse indentation load is applied to the shell.

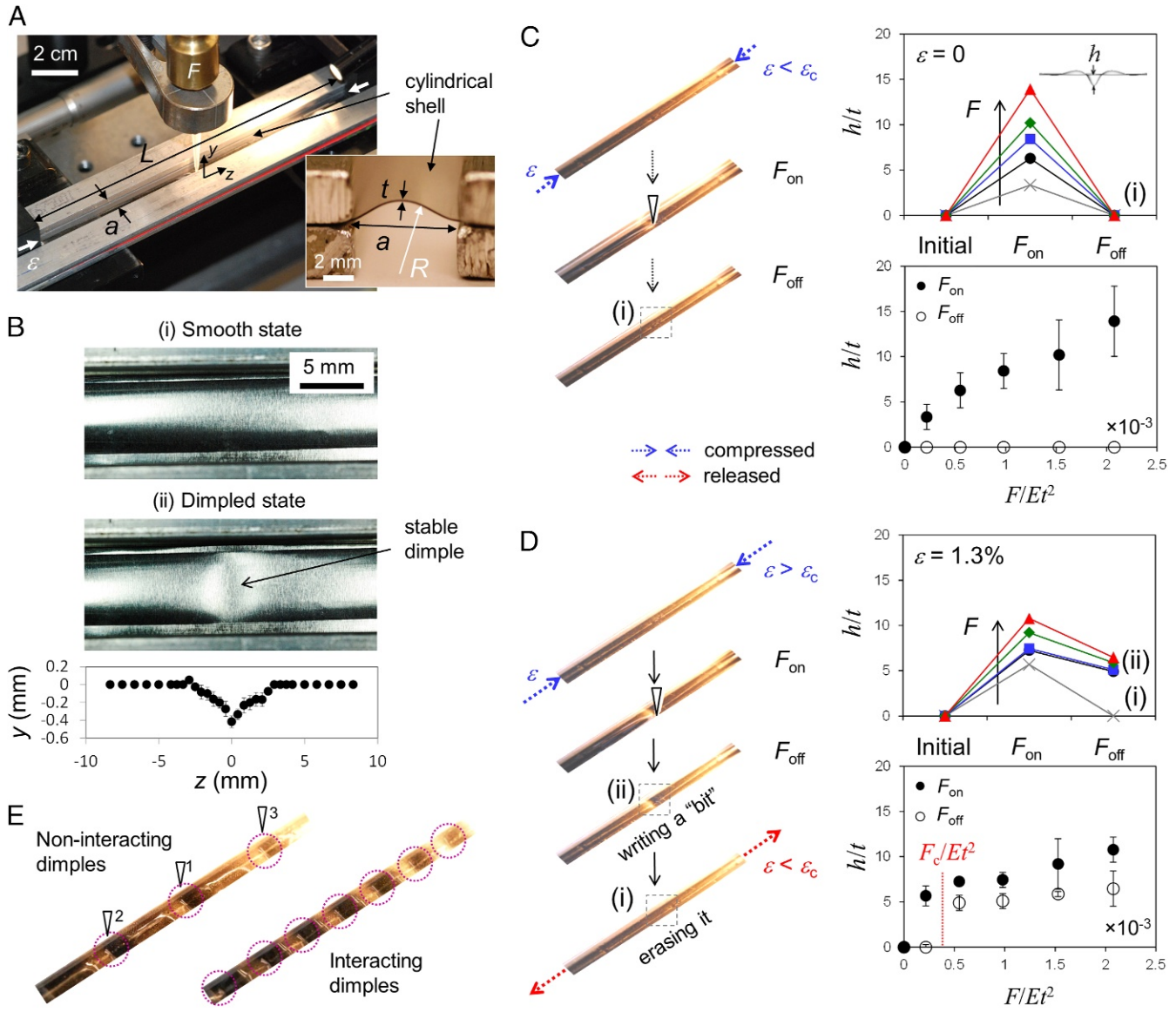

Fig. 2. Localized dimples in a singly curved shell. (*A*) Experimental setup. *Inset* shows an enlarged cross-sectional view of a long weekly curved cylindrical shell made of elastic sheet. (*B–D*) A single dimple can be formed by first applying an axial compressive strain ε to the shell and then pressing an indenter onto the surface under a force F at the location of dimple formation. Two alternative stable states are shown in *B*: a featureless smooth state (*i*) and a dimpled state (*ii*). (*C*) If ε is below a critical value ε_c ($\approx$1% in this case), the shell recovers completely when F is released. (*D*) Conversely, in the case $\varepsilon \geq \varepsilon_c$, the localized dimple persists and is stable even after removal of F when F is above a critical level F_c. This stationary dimple can be further erased by relieving ε. Note that the system is bistable, with no intermediate patterns being observed. Here, h/t is the out-of-plane displacement at the shell center normalized by the shell thickness, and F/Et^2 is the normalized indentation load, with E being the Young's modulus of the shell material. (*E*) Localized multiply dimpled structures. (*Left*) Multiple noninteracting dimples created by indenting a compressed cylindrical shell at different locations that are widely spaced relative to the dimple width. (*Right*) For a large-enough compressive strain, the configuration of the shell allows a stable localized structure with a doublet or higher-order multiplet dimples.

This results in the formation of a stable dimple that persists even after the load is removed, such as can be seen in Fig. 3*B*. Indeed, depending on the applied compressive strain and the magnitude and distribution of the perturbation, we can get one or more dimples that are localized spatially. The states with higher numbers of dimples require a stronger lateral load and have smaller dimple heights, and beyond a second critical strain, there is an invasion transition, wherein the entire shell is replete with localized dimples as shown in Fig. 3*C*.

In Fig. 4*A*, we plot the regions of coexistence of multiply dimpled structures quantified as the normalized height of the middle dimple as a function of the applied compressive strain for structures composed of up to four dimples. Below a critical compressive strain (0.31% in this case), the configuration of the shell does not allow for a stable localized structure. Above the threshold strain, multiply dimpled states coexist and form; their number depends on the applied compressive strain. This is in qualitative agreement with our experimental results as shown in Fig. 4*B*; there are different regimes that show the coexistence of multiply dimpled states.

For a system with existing localized dimpled structures, increasing the compressive strain up to a critical limit increases the amplitude of the existing dimples. Beyond a critical compressive strain, the system evolves dynamically, and additional stable dimples are formed, while the amplitude of original dimples decreases (Fig. 5*A*, *Upper*). This scenario repeats itself as

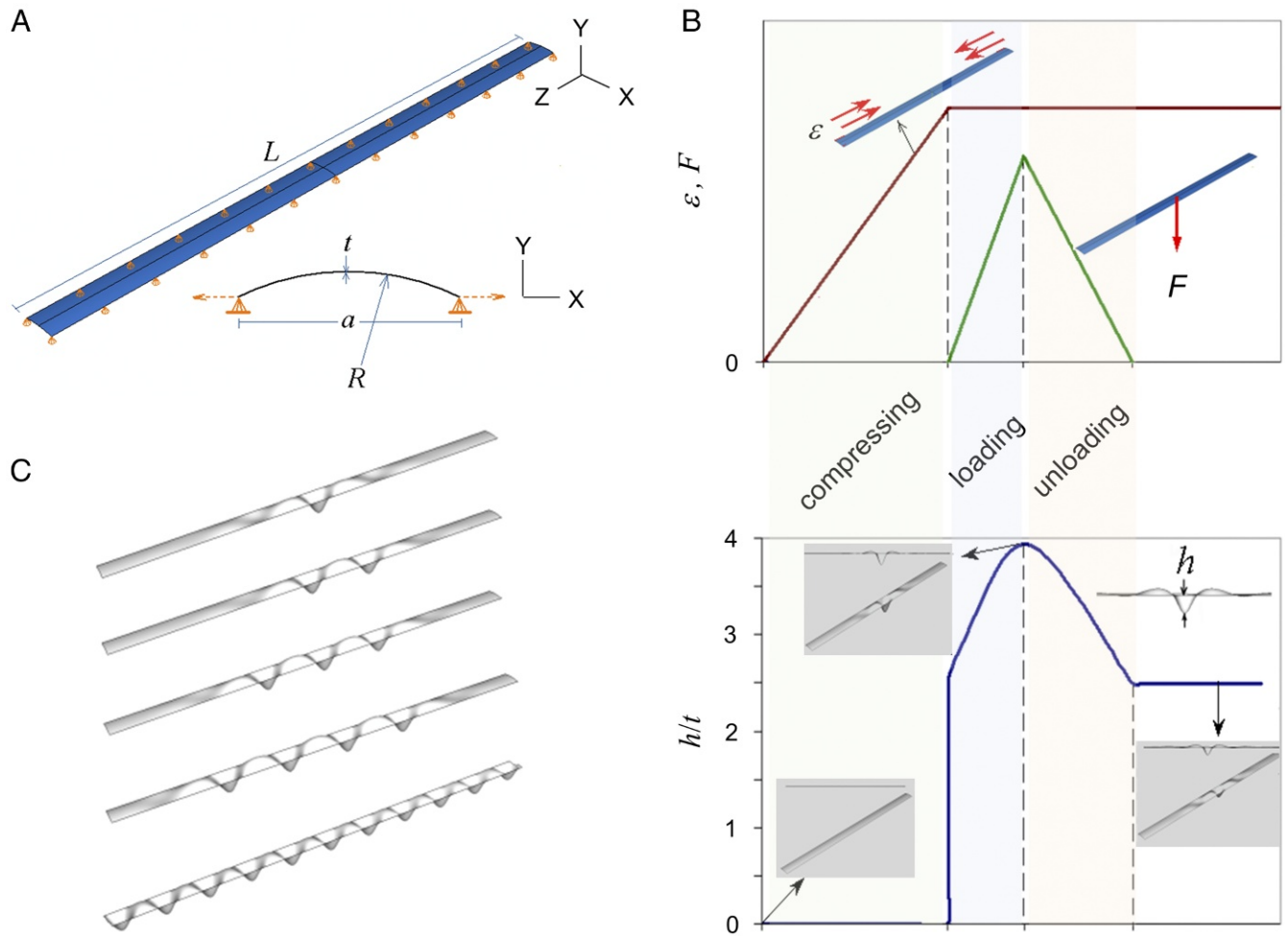

Fig. 3. Formation of stable localized dimples. (*A*) A cylindrical shell with a natural radius of curvature R, thickness t, width a, length L, and Young's modulus E. (*Inset*) Cross-section of the shell and schematic of the edge boundary condition. Two edges of the shell are constrained in the Y direction, while free to slide in the two other principal directions. In all of the simulations, $t/R = 0.01$ and $a/R = 0.4$ if not otherwise mentioned. (*B*, *Upper*) Applied compressive strain and indentation loading. First, a uniform strain ε is induced in the shell by displacing its ends, and second, the shell is perturbed quasistatically using an indentation load F. (*B*, *Lower*) Out-of-plane displacement at the shell center h normalized by the shell thickness t as a function of F. We see that the localized dimple persists and is stable even after removal of F. *Insets* show the deformed configuration of the system at different stages of loading (out-of-plane displacements are magnified by a factor of 25). In this case, $\varepsilon = 0.337\%$ and F/Et^2 (normalized indentation load) $= 10^{-3}$. (*C*) The number of localized dimples depends on the applied ε and the magnitude of F. For a large-enough compressive strain and/or indentation load, the system is fully populated by stationary localized dimples as shown at the bottom. In this simulation, $\varepsilon = 0.46\%$ and $F/Et^2 = 0.56 \times 10^{-3}$.

the applied strain is increased even further. The system always keeps its initial symmetry, with two evolution paths depending on whether the number of initial dimples is odd or even. In contrast, on decreasing the applied compressive strain, all of the dimples disappear simultaneously when the strain decreases below a critical value, which depends weakly on the number of dimples (Fig. 5*A*, *Lower*). Fig. 5*B* shows the corresponding experimental results, which exhibit behavior similar to the theoretical predictions. We see that gradual compression of the existing localized dimpled structure induces sharp saw tooth-like oscillations in the height of the original dimple. The sharp height drops are at critical strain values (Fig. 4*B*), and at each transition, two neighboring new dimples are formed simultaneously. However, when the strain is reversed, the dimple height decreases monotonically, thus revealing a pronounced hysteresis between loading and unloading paths.

To understand the dynamical evolution of the localized dimples, we also varied the applied body force for a system with existing localized dimpled structure (*SI Appendix*, Fig. S1*A*). When the body force is less than a critical limit, the system behavior is insensitive to the magnitude of body force. As the body force is increased beyond this critical limit, the dimpled configuration invades the entire system (i.e., the entire system is replete with stable localized dimples as shown in Fig. 3*C*) at a constant velocity that depends on the applied compressive strain (*SI Appendix*, Fig. S1*B*).

When the lateral extent of the elastic shell is not quasi-1D, the localized patterns are no longer restricted to line-like Braille dimples. Instead, one can "write" as on a 2D substrate. As an example, when we use a wide shell of constant natural radius of curvature that is clamped along the edges, the localized structures generated by lateral load can form complex 2D patterns (*SI Appendix*, Fig. S2).

Discussion

Our study builds on and complements work in abstract spatial dynamical systems that suggest the possibility for localized structures (6, 7, 16, 17, 19). While these studies have inspired the notion that these localized structures could serve as bits for information storage in lattice-free continuum settings that are

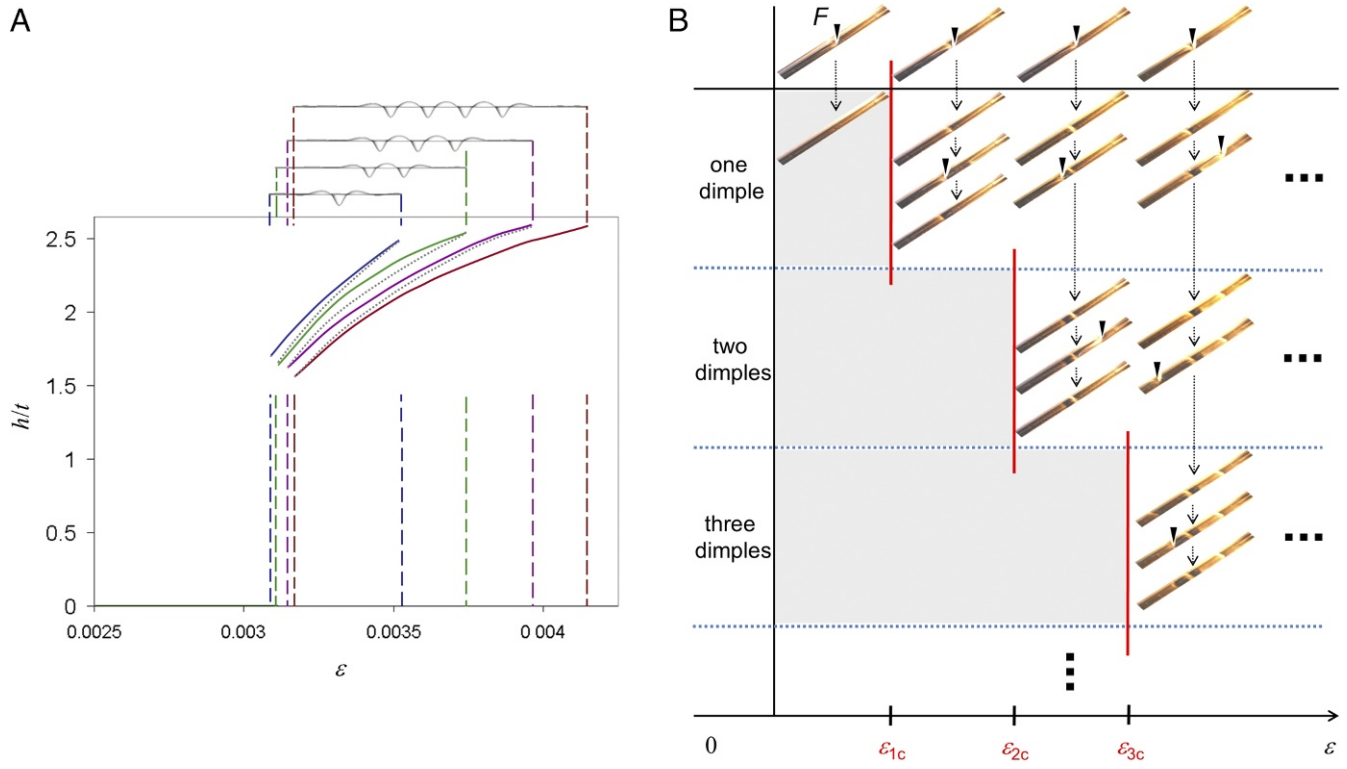

Fig. 4. Multiply dimpled states. (*A*) Regions of coexistence of multiply dimpled structures. The height h of a middle dimple (normalized by the shell thickness t) is plotted as a function of the applied compressive strain ε. The solid and dotted lines correspond to stable and unstable homogeneous solutions, respectively. (*B*) Experimental analog to the simulations presented in *A*, revealing various configurations of multiple noninteracting localized dimples shaped by indenting a cylindrical shell in different locations along its top surface. The number (N) of stable localized dimples that can form strongly depends on the applied compressive strain ε. We see that there is a different critical compressive strain value ε_{Nc} for each number of dimples, below which the configuration of the shell does not allow stable localized structures with a higher number of dimples. There are also regions of coexistence of multiply dimpled structures; for example, when $\varepsilon \gtrsim \varepsilon_{3c}$, we see that multiply dimpled states (up to three) form and coexist. In this experiment, F/Et^2 (normalized indentation load) $\approx 1.0 \times 10^{-3}$, $\varepsilon_{1c} \approx 1.0\%$, $\varepsilon_{2c} \approx 1.9\%$, and $\varepsilon_{3c} \approx 2.6\%$.

naturally described as continuum fields (8), there are few experimental systems where this has been directly realized. Using experiments and computations, we have shown how a featureless elastic plate can serve as a substrate for reversible elastic memories that take the form of Braille-like dimples. Unique to our system is the role of geometric nonlinearities that drive pattern formation, making our results fairly robust and easy to realize. Indeed, since the dimples form in response to a localized indenter in the presence of an applied compressive strain and a body force, we have shown that reprogrammable Braille is relatively easy to realize. Since the geometrical nonlinearities in thin shell-like structures are dependent only on the separation of scales between the thickness of the structure and the lateral dimensions, independent of the absolute scale, and the nature of the material as long as it is linearly elastic, these localized Braille-like structures should be realizable experimentally on nano-, micro-, meso-, and macroscales and might serve as the basis for mechanical memories on multiple scales.

Materials and Methods

A thin sheet of transparent polyester film (3M OHP Transparency Film; thickness $t \approx 130$ μm) or stainless steel shim (Trinity Brand Industries, Inc.) was used to create a long, weakly curved cylindrical shell. The sheet was first cut into long, narrow strips with length L and width W, where $L \gg W \gg t$, each of which was then slightly curved along its entire width by mounting it on a long steel rod of diameter $2R$ larger than W. In the case of the polyester film, the mounted strip was subjected to thermal treatment in an oven at 180°C for about 20 min followed by rapid cooling to room temperature to form a singly curved thin shallow shell of arch width a and radius of curvature R ($t/R \approx 0.01$, $a/R \approx 0.54$). In the case of the stainless steel, the mounted strip was hard pressed to form a cylindrical shell, which has $t/R \approx 0.004$ and $a/R \approx 0.46$.

To constrain the shell along its long edges, a small portion of the edges was bent slightly outward to form an omega (Ω)-like shape, and each of these edge portions was sandwiched between two aluminum plates with just enough gap between them, which serves as a guide rail to let it slide freely (Fig. 2*A*). Furthermore, the two parallel identical guide rails were spaced apart a distance approximately the arch width of the shell. The two circumferential ends of the shell were mounted on rigid frames attached to linear translation stages (Newport Corp.), which allow axial displacements with a precision of a few hundreds of micrometers.

As illustrated in Fig. 2*A*, the longitudinal strain ε was induced in the shell by incrementally displacing its ends in the opposing axial direction, and a localized transverse indentation load was applied by pressing the shell with a conical tip (tip diameter ≈ 0.7 mm $\ll a$) under a dead weight load. In this study, ε was varied in the range from 0 to 0.08 with an increment $\Delta\varepsilon$ of ∼0.0036 (compression being taken as positive), while other parameters were kept constant unless otherwise specified. All experimental images were obtained with a digital camera (Nikon D80) equipped with a zoom lens (Sigma 105-mm f/2.8 EX DG Macro lens), except for those in Fig. 2*B*, which were taken by zoom stereo microscope (Nikon SMZ800). The amplitudes of the dimples, as shown in Figs. 2 and 5, were measured with a homebuilt setup that enables the measurement with accuracy within a few tens of micrometers.

A commercial package, ABAQUS, was used to solve the 3D equations of elasticity. Four-node quadrilateral thin shell elements with reduced integration (element type, S4R) and a large deformation formulation were used in all simulations, with five integration points through the shell thickness. A mesh sensitivity study was carried out to ensure that the results are minimally sensitive to the element size. The free mesh scheme available in the ABAQUS software was used in the computational model with no initial geometric or material imperfection. The local instabilities in the structure

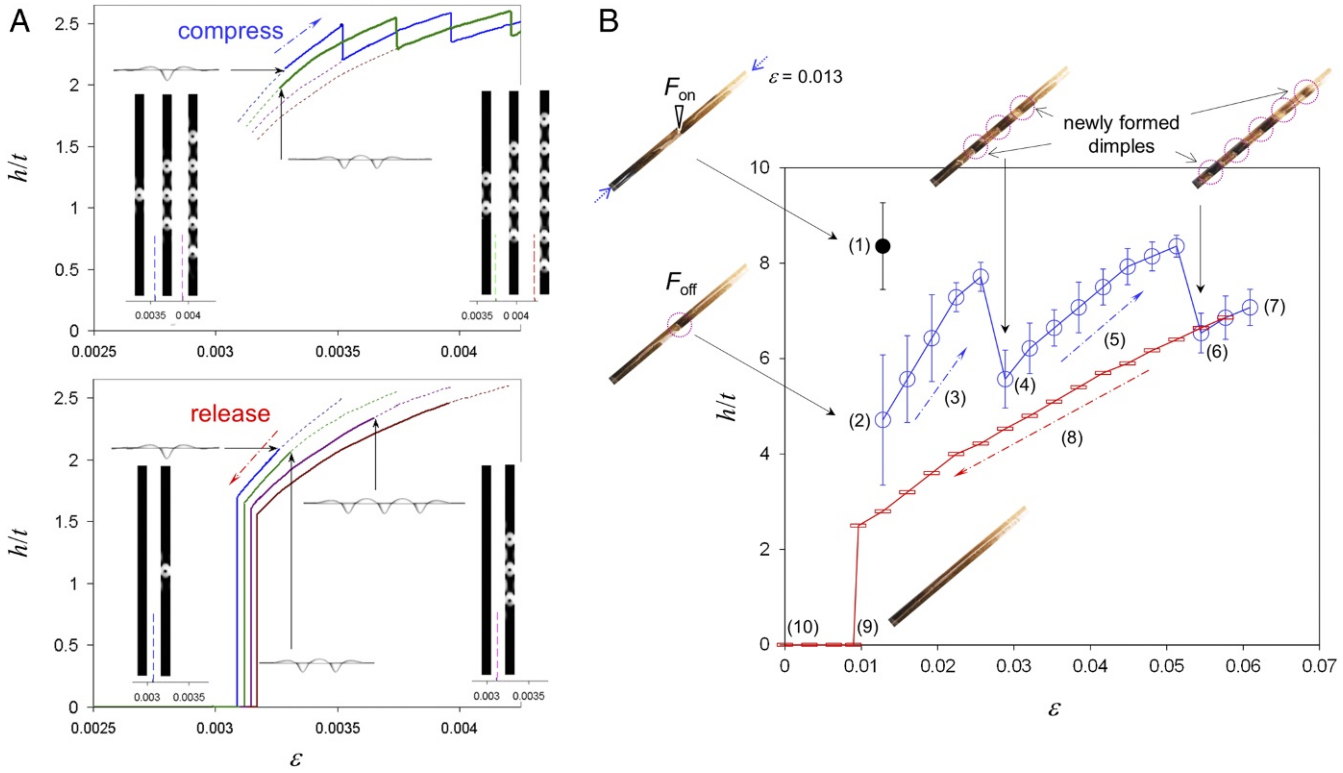

Fig. 5. Evolution of localized dimples. (*A*) The dimpled structures evolve with changing applied compressive strains ε. (*Upper*) Increase in ε initially leads to an increase in the height h of a single dimple (normalized by the shell thickness t). At a critical value of ε, the shell dynamically evolves as two new dimples are born; simultaneously, their height decreases. This scenario repeats itself as ε is increased further. Two distinct evolution paths are revealed depending on whether the number of dimples is even or odd. (*Lower*) Decrease in ε leads to reduction of the dimple heights followed by the disappearance of one at a critical limit. *Insets* show actual results of the simulations. In lateral views shown as *Insets*, the out-of-plane displacements are scaled up by a factor of 25. (*B*) Experimental bifurcation diagram as a function of ε, in qualitative agreement with the simulation results shown in *A*. The cylindrical shell is compressed uniaxially up to a strain of $\varepsilon = 1.3\%$ (above a threshold level, $\varepsilon_c \approx 1\%$), and a normalized indentation load of $F/Et^2 \approx 1.0 \times 10^{-3}$ is applied to the shell (*1*). The load is then released, leading to the formation of a localized stable dimple (*2*). Subsequently, ε is varied in a stepwise fashion with an interval of ≈0.36%: first, increasing (compressing) to a certain value at which the dimpled structure is composed of up to five dimples (from *2* to *7*) and second, decreasing (releasing) back to zero (from *7* to *10*). *Inset* shows the dimpled structures corresponding to the numbered labels.

were captured using a stabilizing mechanism based on automatic addition of volume-proportional damping, which was decreased systematically to ensure that the response was insensitive to this change. It is worth pointing out that these numerical simulations can account for instabilities and have been validated against experiments to probe the medium-to-large deformation regime (20, 21).

Acknowledgments. We thank Christophe Riera and John W. Hutchinson for many fruitful discussions. This work was partially supported by National Science Foundation (NSF) Grants DMR 14–20570 (to J.Y.C. and L.M.) and DMR 33985 (to J.Y.C. and L.M.), NSF Grant CMMI-0736019 (to A.V.), Air Force Office of Scientific Research Grant FA 9550-10-1-0145 (to A.V.), NSF Grant 1149750 (to A.V.), Qatar Foundation's National Priorities Research Program Grant 5-068-2-024 (to A.V.), and the MacArthur Foundation (L.M.).

1. Kandel ER (2001) The molecular biology of memory storage: A dialogue between genes and synapses. *Science* 294:1030–1038.
2. Chappert C, Fert A, Van Dau FN (2007) The emergence of spin electronics in data storage. *Nat Mater* 6:813–823.
3. Raman KV, et al. (2013) Interface-engineered templates for molecular spin memory devices. *Nature* 493:509–513.
4. Badzey RL, Zolfagharkhani G, Gaidarzhy A, Mohanty P (2004) A controllable nanomechanical memory element. *Appl Phys Lett* 85:3587–3589.
5. Wuttig M, Yamada N (2007) Phase-change materials for rewriteable data storage. *Nat Mater* 6:824–832.
6. Pomeau Y (1986) Front motion, metastability and subcritical bifurcations in hydrodynamics. *Physica D* 23:3–11.
7. Coullet P, Riera C, Tresser C (2000) Stable static localized structures in one dimension. *Phys Rev Lett* 84:3069–3072.
8. Coullet P, Riera C, Tresser C (2004) A new approach to data storage using localized structures. *Chaos* 14:193–198.
9. Knobloch E (2015) Spatial localization in dissipative systems. *Annu Rev Condens Matter Phys* 6:325–359.
10. Timoshenko S, Woinowsky-Krieger S (1959) *Theory of Plates and Shells* (McGraw-Hill, New York).
11. Kebadze E, Guest SD, Pellegrino S (2004) Bistable prestressed shell structures. *Int J Sol Struct* 41:2801–2820.
12. Giomi L, Mahadevan L (2012) Multi-stability of free spontaneously curved anisotropic strips. *Proc R Soc A* 468:511–530.
13. Arza A, Schroll R, Cerda E (2013) Near and far from the threshold analysis of rectangular elastic plates. *J Phys A Math Theor* 46:135203.
14. Cross MC, Hohenberg PC (1993) Pattern formation outside of equilibrium. *Rev Mod Phys* 65:851–1112.
15. Homburg AJ (1996) *Global Aspects of Homoclinic Bifurcations of Vector Fields* (American Mathematical Society, Providence, RI).
16. di Bernardo M, Budd CJ, Champneys AR, Kowalczyk P (2008) Qualitative theory of non-smooth dynamical systems. *Appl Math Sci* 163:47–119.
17. Devaney RL (1977) Blue sky catastrophes in reversible and Hamiltonian systems. *Indiana Univ Math J* 26:247–263.
18. Cai S, Breid D, Crosby AJ, Suo Z, Hutchinson JW (2011) Periodic patterns and energy states of buckled films on compliant substrates. *J Mech Phys Solids* 59:1094–1114.
19. Lee KJ, McCormick WD, Ouyang Q, Swinney HL (1993) Pattern formation by interacting chemical fronts. *Science* 261:192–194.
20. Vaziri A, Mahadevan L (2008) Localized and extended deformation of elastic shells, *Proc Natl Acad Sci USA* 105:7913–7918.
21. Nasto A, Ajdari A, Lazarus A, Vaziri A, Reis PM (2013) Localization of deformation in thin shells under indentation. *Soft Matter* 9:6796–6803.